



DYNAMIC RESPONSE OF HIGH-RISE STEEL STRUCTURES UNDER SUCCESSIVE STRONG EARTHQUAKE SEQUENCES

S. Yuan⁽¹⁾, Y. Sun⁽²⁾, T. Takeuchi⁽³⁾

⁽¹⁾ Graduate student, Graduate school of engineering, Kobe University, Japan, yuanshiyu0510@gmail.com

⁽²⁾ Professor, Graduate school of engineering, Kobe University, Japan, sun@person.kobe-u.ac.jp

⁽³⁾ Assistant Professor, Graduate school of engineering, Kobe University, Japan, takeuchi_t@person.kobe-u.ac.jp

Abstract

In the last 20 years, some insights have been provided about the response of steel structures under successive earthquake seismic sequences or mainshock-aftershock (MSAS) seismic sequences. The main outcome concentrates on that the aftershocks increase seismic response parameters such as interstory drift ratio (IDR), residual drift ratio, and certain damage indexes. However, the dynamic response features of high-rise steel moment-resisting frame (SMRF) structures under successive strong earthquake sequences have not yet been examined.

In this study, the maximum and residual IDRs of a high-rise SMRF under artificial MSAS seismic sequences were calculated. A 2-D model of a 40-story 4-bay SMRF was designed following the criteria during 80s~90s in Japan. The H-shape steel beam and square hollow steel column members were modeled by fiber-based models. A non-linear stress-strain model considering the beam-columns' strength and stiffness deterioration due to the local buckling was adopted. 6 ground motion accelerogram records, including 3 recorded ground motions and 3 artificial ground motions, were selected for the time history analysis. For each ground motion, 15 intensity combinations of the main-event with the intensity factor in the range of 1 to 3 and after-event with the intensity factor in the range of 0.5 to 3.6 were arranged. The intensity factor "1" was equivalent to the Level 2 ground motion intensity for the safety limit in Japanese design code.

The after-event maximum IDR ($A R_{max}$) was compared with the predicted one ($p A R_{max}$), which defined as a summation of the main-event residual IDR ($M R_r$) and the maximum IDR under a single event equals to the after event ($S R_{max}$). The $p A R_{max}$ had $\pm 30\%$ agreement with the $A R_{max}$ regardless of taking the deterioration into consideration or not, except for one case "J-Hachi3+3.6". At this case, the $A R_{max}$ on the first story in the analysis considering the deterioration was 1.59 times of $p A R_{max}$, while that ignoring the deterioration was 0.99 times of $p A R_{max}$. In this case, the permanent residual IDR occurred during the main event triggered the deterioration of columns at 1 floor during the after event, resulting in a story collapse.

These results demonstrate that the summation of $M R_r$ and $S R_{max}$ could be a simple prediction approach for $A R_{max}$ of high-rise (SMRF) structures under successive strong earthquake sequences. However, under a certain extreme condition, this prediction approach would neglect the possibility of serious non-linear response behaviors such as a story collapse.

Keywords: *Successive Strong Earthquake Sequences, Deterioration, Interstory Drift Ratio*



1. Introduction

It is a general knowledge that a severe mainshock follows with strong aftershocks. As an example of such mainshock-aftershock (MSAS) sequences, the Chi-Chi earthquake ($M_L=7.3$) struck the central region of Taiwan on Sept. 21 1999, and two strong aftershocks of $M_L=6.8$ occurred about 30 hours and 127 hours after the mainshock [1]. Another type of consecutive earthquakes is that the offshore megathrust earthquake triggers strong aftershocks and new events, such as the 11 March 2011 Tohoku earthquake ($M_w=9$) in Japan, followed with a large number of aftershocks or triggered events [2]. 5 aftershocks or triggered events have a magnitude larger than $M_j=7$ (the Japan Meteorological Agency magnitude). Furthermore, another rare case such as the Kumamoto earthquakes in April 2016 is characterized by a strong fault-type foreshock ($M_w=6.2$) and an even stronger mainshock ($M_w=7.0$) [3]. Successive strong ground motions can be observed during such earthquake sequences, usually separated by a short time blank such as hours or days. Thus, the damaged structures may suffer further damage or become completely unusable at the end of the after events.

There have been several researches about the response of engineering structures subjected to the successive ground motion sequences. Some of those focused on the nonlinear response of single-degree-of-freedom (SDOF) systems [4-9], while others investigated the nonlinear response of multiple-degree-of-freedom (MDOF) systems such as steel frame models [10-13], RC frame models [14-16], et al. The main outcome by the researches on SDOF systems [4-9] concentrates on that the consecutive earthquake sequences demands larger inelastic displacement or other damage indexes. Empirical expressions were proposed for the prediction of the force reduce factor, the inelastic displacement ratio and the interstory drift ratio (IDR) for SDOF systems under artificial ground motion sequences [4-6]. However, some researches have shown differences between the response of equivalent SDOF systems and MDOF frame models (such as Ref. [10]).

In addition, the research on high-rise steel moment-resisting frame (SMRF) structures under such earthquake sequences is still considered insufficient. Li and Ellingwood [11] studied the response of 2D models of 9-story and 20-story SMRF frames, in which the connections were modelled by a moment-rotation relationship that took the brittle fracture of the connection welds into account. Ruiz-Garcia and Negrete-Manriques [12] adopted 4-story, 8-story and 12-story SMRFs as research targets and modeled those frames as half models due to symmetry in the building plan. The elements in these research are mostly modeled as plastic-hinge models. The moment-rotation hysteric rules for hinges, such as Takeda-type ones, were usually modeled after the steel specimens' tests under constant axial loading and reversed cyclic lateral loading, which ignored the changing of axial load level. However, the seismic axial loads may raise to a very high level in columns for the high-rise SMRFs under strong ground motions [17]. Proper modelling methods are required for investigating the effect of strong earthquake sequences to the response of high-rise SMRFs.

Meanwhile, the modelling method is improving along with the discoveries on the SMRFs' dynamic response. Kim et al. [18] pointed out that the damage of high-rise SMRFs tends to concentrate on the lower floors due to the effect of the P- Δ effect. Bai et al. [19] introduced a fiber-based model for steel beam-column elements to incorporate the strength deterioration due to the local buckling and conducted IDA (short for Incremental Dynamic Analysis [20]) for 20-story 30-story and 40-story SMRFs, suggested that when considering the structural members' deterioration triggered by local buckling, the maximum IDRs were larger at high level of ground motion intensity than those when the deterioration was ignored.

In this research, a 40-story high-rise SMRF was designed. Structural members' sections were modelled by fiber method, in which the seismic axial load changing can be directly reflected in fibers' stress-strain hysteric response. The constructive stress-strain relationships [19], considering or ignoring strength deterioration triggered by local buckling, were adopted to specify the difference on the response of the target model respectively. 84 artificial successive ground motions with varied intensity combinations were generated from 3 as-recorded ground motions and 3 artificial ones. Time history analyses of the target model under these successive ground motion sequences have been conducted and the maximum and residual IDRs were compared between the models considered or ignored the deterioration. A prediction approach for the aftershock IDR response was suggested and the prediction accuracy for the after-event maximum IDR (AR_{max}) was checked for all the cases.



2. Structural Model and Ground Motions

2.1 Constructive Stress-Strain Relationship for Steel Fibers

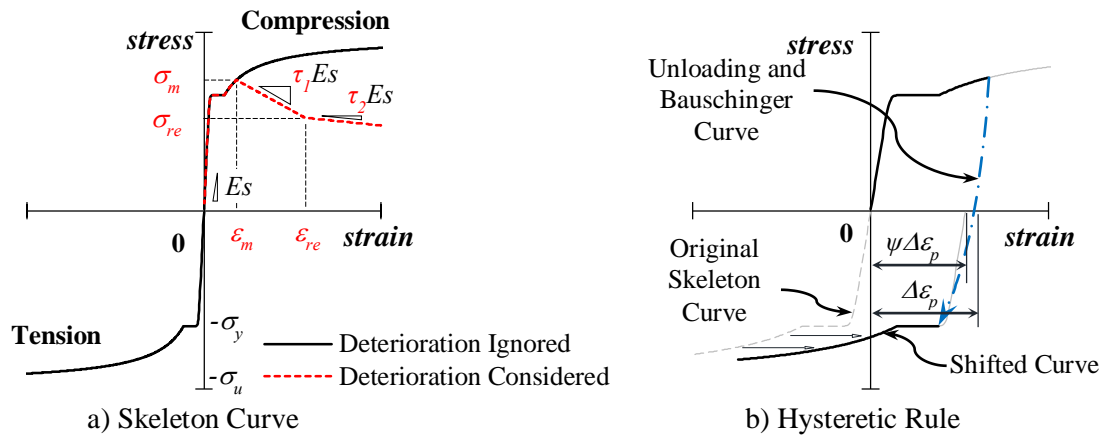


Fig. 1 – Stress-strain relationship for steel element fiber

The analysis was conducted by a 2-D nonlinear analysis program developed by Kawano and Warner [21]. The nonlinear stress-strain model adopted in this research, considering the beam-columns' strength and stiffness deterioration due to the local buckling [19], is shown in Fig. 1. The skeleton curve includes two Menegotto-Pinto curves for the elastic branch and the plastic branch. The strength deterioration triggered by local buckling is presented by a negative slope in compression side. The negative slope started from the decreased ultimate stress σ_m . Control points (σ_m, ϵ_m) and $(\sigma_{re}, \epsilon_{re})$ on the negative slope are determined by the width-to-thickness ratio of the steel material. The details for the calculation of these critical parameters can be found in Ref. [19]. In order to specify the influence of the local-buckling-triggered deterioration and to avoid complication, other reasons for the deterioration, such as the fracture of welded connections et al., were ignored.

The hysteresis rule is based on the proposal of Kato et al. [22]. The skeleton curve part is separated into the compression and tension skeleton curves which are connected by the unloading and Bauschinger part. As shown in Fig. 1(b), when the fibers' strain has reached a certain value larger than the yield strain, the skeleton curve on the reverse side will shift to illustrate the accumulation of plastic strain. And the stress-strain path to the reverse side will follow the unloading and Bauschinger curve. The unloading and Bauschinger curve is defined by a Menegotto-Pinto curve starting from unloading point and pointing to the experienced stress point on the shifted curve of the reverse side. The shift amount is controlled by a parameter ψ that is the ratio of the strain shifting value $\psi\Delta\epsilon_p$ relative to the experienced plastic strain $\Delta\epsilon_p$ during the previous loading procedure. In this research, the value of ψ is set to 0.8, as suggested by Meng et al. [23].

2.2 Modelling of Beam-column Members and the High-rise SMRF

The sections of beam-column elements were divided into fiber elements. As shown in Fig. 2(a) and (b), the web was divided into 8 fibers and the flange was divided into 2 fibers for both the column and beam sections. The floor slab, which affects the stiffness of the H-section steel beam, was also modeled within the section of beam elements. The width of the slab considered was 1/5 (1.6 meters) of the span (8 meters), the thickness was 150 mm, and the slab section was divided into 6 fibers. The constitutive stress-strain relationship for the concrete floor slab is Popovics model [24]. The tensile stress is set as 0. The unloading part is defined by a straight line that connects the unloading start point and half of the experienced strain at the previous loading progress.

Two plastic hinge regions were constituted at both ends of a beam-column member, as shown in Fig. 2(c). The length of hinge region equals to the cross-sectional depth. These hinge regions are also expected to perform the post-buckling large deformation.

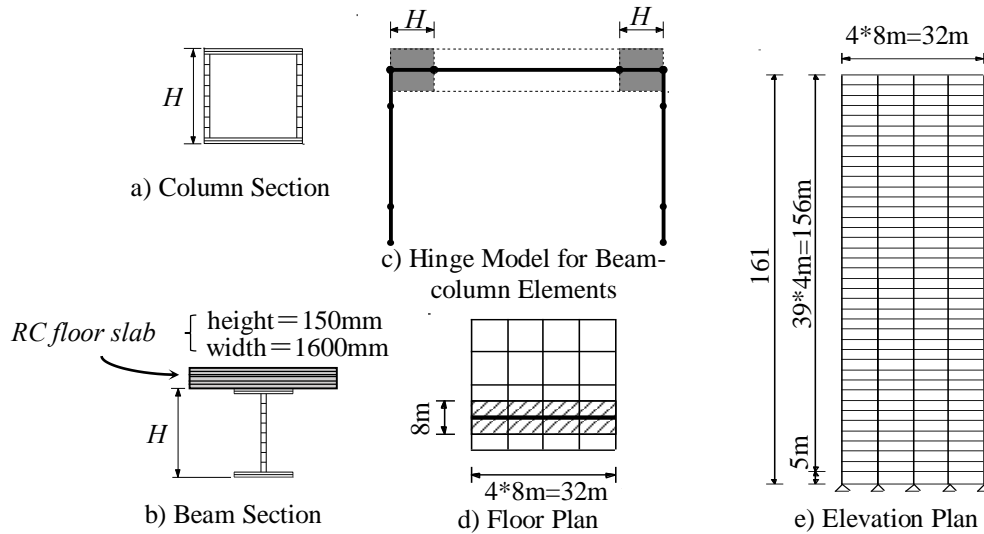


Fig. 2 – Modeling details of the target high-rise SMRF structure

A 2-Dimensional model of a 40-story 4-bay SMRF was designed following the criteria during 80s~90s in Japan. Fig. 2(d) and (e) shows the building plan. The shaded area in Fig. 2(d) is the load bearing area for the 2-D planar frame. The vertical load was 7.84 kN/m^2 for all layers. The tension strength of steel material is 490 N/mm^2 for all the beam-column elements. All beam and column members belong to rank FA, which means high ductile steel members in current Japanese code. The natural period of the model is 4.88 sec.

2.3 Ground Motions

In this study, artificial approach was adopted to generate successive ground motions. 6 ground motion accelerogram records, included 3 recorded ground motions (provided by BCJ) and 3 artificial ground motions (provided by JSCA), were selected as the original waves for generating successive ground motions. The duration of 3 recorded records were extended to 60 seconds by adding 0 acceleration time to the original record. The basic information of these ground motions can be seen in Table 1.

14 sets of the first (main event) and the second (after event) seismic intensity combinations were arranged as shown in Table 2. The ground motion with a scaling factor $\phi=1$ is equivalent to the Level 2 intensity for the safety limit in Japanese code. 3 recorded ground motions were normalized to $\text{PGV}=50 \text{ cm/s}$, and 3 JSCA ground motions were amplified 1.25 times of the original ones. 60 seconds of 0 acceleration time were added to the end of the first wave as the blank time between the main event and the after event. Another 60 seconds of 0 acceleration time was added to the end of the second wave for the damped free vibration. An input case is tagged as “wave name” & “ $\phi_M + \phi_A$ ”, ig. JscHachi1+1.2 stands for an input wave constructed by a JscHachi with $\phi=1$ as the main event and a JscHachi with $\phi=1.2$ as the after event.

Table 1 – Basic information of the original ground motions with scaling factor $\phi=1$

Record Name	Type	Original Length (sec)	PGA* (cm/s/s)	PGV* (cm/s)
El Centro NS		53.76	510.0	50
Hachinohe NS	recorded	51.00	333.7	50
Taft EW		54.40	496.9	50
JscHachi		60.00	436.3	61.0
JscKobe	artificial	60.00	366.3	66.1
JscTohk		60.00	476.3	68.3

*Values after the ground motions been scaled to Level 2.

Table 2 – Combinations of scaling factors for main event ϕ_M and after event ϕ_A

Series	1+x	2+x	3+x
$\phi_M + \phi_A$	1+0.5	2+0.5	3+0.5
	1+0.8	2+1.0	3+1.0
	1+1.0	2+1.6	3+2.4
	1+1.2	2+2.0	3+3.0
		2+2.4	3+3.6

* All 6 original ground motions following these 14 sets of $\phi_M + \phi_A$.

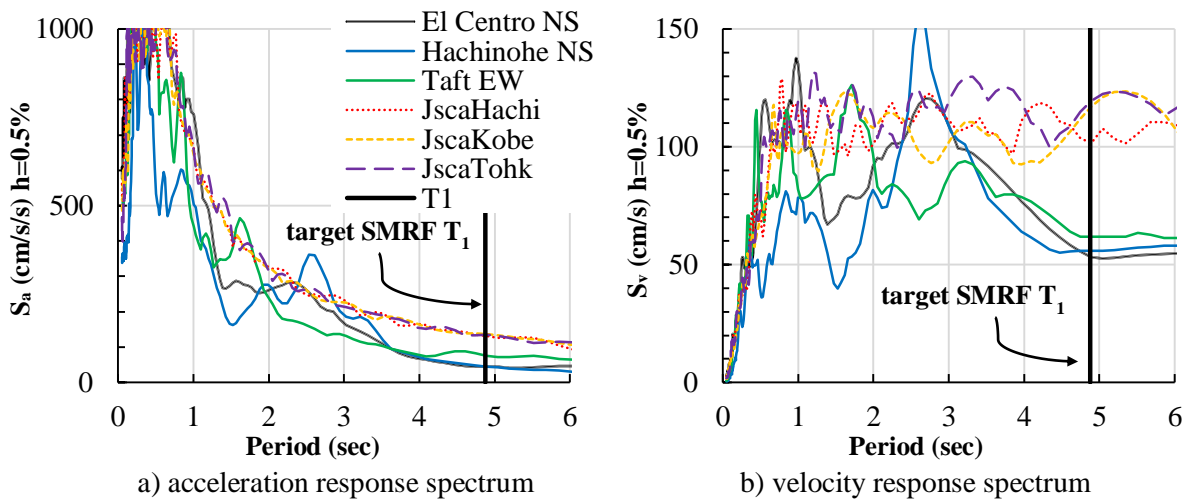


Fig. 3 – The response spectrum of Level2-normalized ground motions

Fig. 3 shows the acceleration and the velocity response spectrum of all 6 waves normalized to Level 2. The JSCA waves are stronger than the recorded waves in the aspect of the acceleration and the velocity spectrum values at the natural period of the 40-story SMRF model (4.88sec). The difference of input waves enhanced the diversity of the intensity match of successive seismic sequences. All dynamic analyses were performed with the Newmark- β method ($\beta=1/4$). The time increment was 0.02 second. The damping type was Rayleigh damping for the 1st and 2nd normal mode (damping ratio $h=2\%$). P- Δ effect was considered.

3. Response Results and Discussion

3.1 Response Maximum IDR and Residual IDR under Single Events

Response analyses under scaled single events were conducted to handle the performance of the target model. The original waves were scaled with a series of scaling factors. The specific scaling factors ϕ_S were set as 0.5, 0.8, 1, 1.2, 1.5, 1.6, 2, 2.4, 2.5, 3, 3.6, including all the ϕ_A values in Table 2. The response maximum IDR (R_{max}) and residual IDR (R_r) ($\phi_S=0.5, 1, 1.5, 2, 2.5, 3, 3.6$ for 6 original waves) are shown in Fig. 4. As mentioned before, the original waves have different intensity for the target model. Hence, R_{max} and R_r under the recorded waves are relatively lower than the JSCA-wave cases.

The influence of deterioration also varied according to the input intensity. No difference can be confirmed on R_{max} and R_r in the recorded-wave cases (Fig. 4a-c), whether considering the deterioration (de-on) or not (de-off). However, in the JSCA-wave cases (Fig. 4d-f), when the scale factor $\phi_S \geq 2.5$, the de-on R_{max} and R_r curves slightly separated from the de-off curves. Such phenomenon was also confirmed in the IDA (short for Incremental Dynamic Analysis [20]) results for 20- and 30-story SMRF models in another research [24]. Response results under single event inputs were also used for the comparison with the equivalent-after-event response of the target model during successive ground motions.

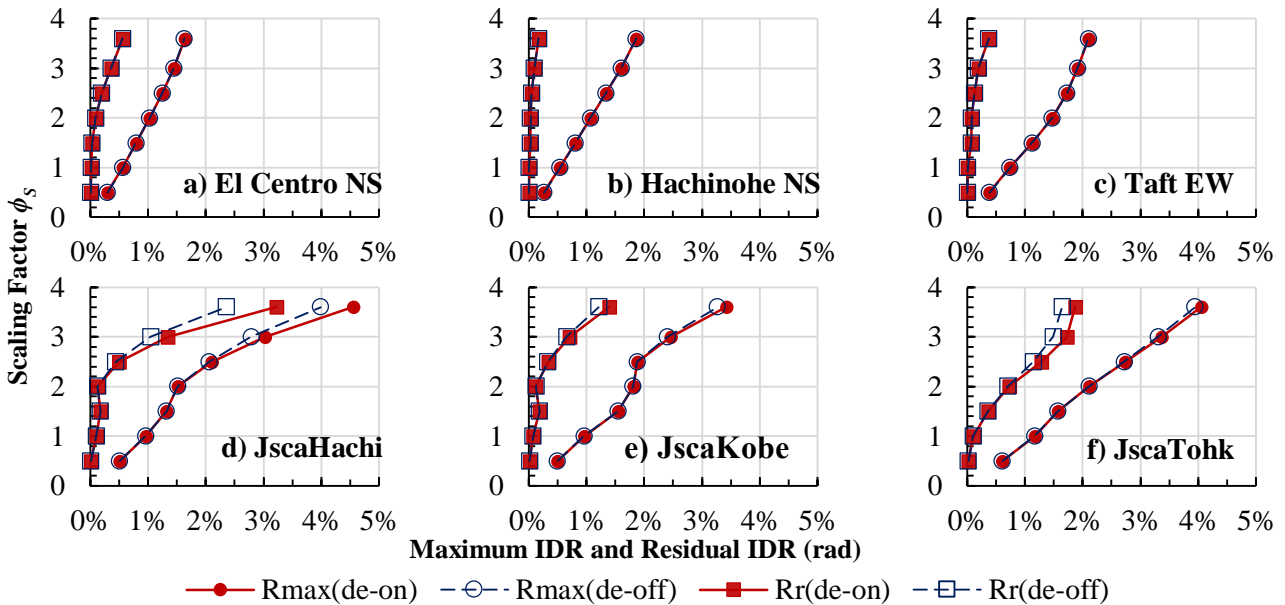


Fig. 4 – Maximum and residual IDR under single scaled seismic input ($\phi_s=0.5, 1, 1.5, 2, 2.5, 3, 3.6$)

3.2 Response Results under Successive Ground Motions

As representative examples, the time histories of model's roof drift displacement under JscaHachi 1+0.5, 1+1.2, 3+0.5 and 3+3.6 are shown in Fig. 5. Obviously, maximum roof drift displacement demands and permanent displacement demands were related to the main-event after-event seismic intensity combinations. The consideration of deterioration also influenced the drift displacement in different level.

For the cases JscaHachi1+0.5 (Fig. 5a) and 1+1.2 (Fig. 5b), no difference can be confirmed despite the consideration of deterioration because the main event and the after events of both are not strong enough. For the case JscaHachi3+0.5, a slightly difference emerged between the de-on line and the de-off line during 0-120sec (the main event JscaHachi with $\phi=3$). This response deformation shift can also be found in Fig. 4d, which infers that the consideration of deterioration slightly influenced the model's response under the main event input JscaHachi with $\phi=3$. The roof drift deformation difference remained during 120-240sec (the after event JscaHachi with $\phi=0.5$). It proved that even the aftershock was not strong enough to drive the model into

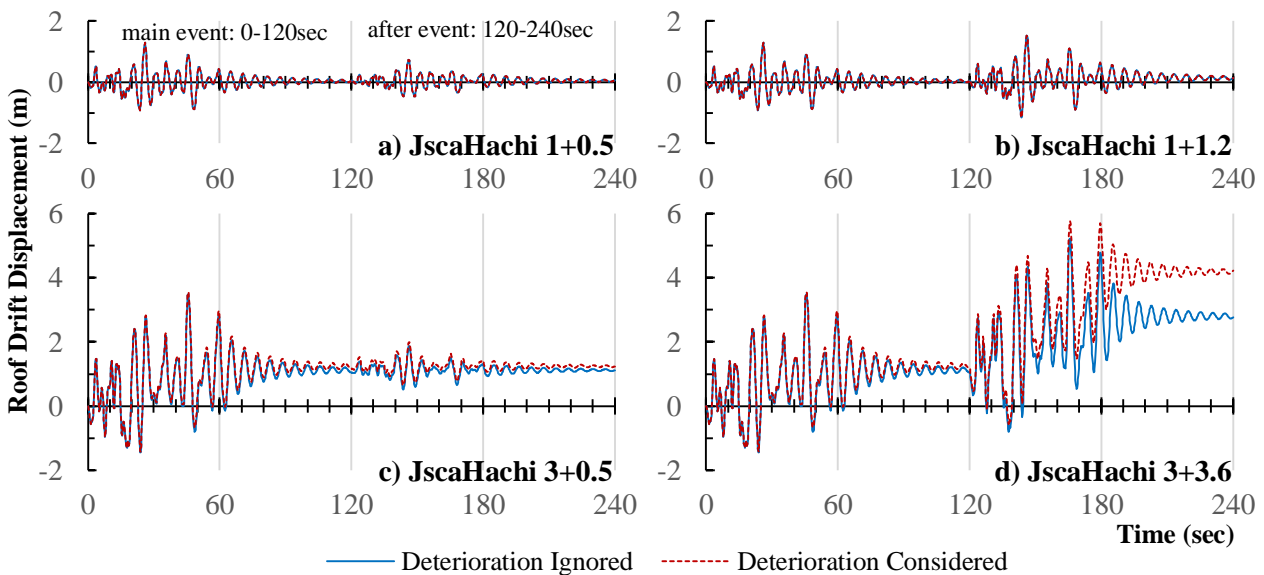


Fig. 5 – Time History of Roof Drift Displacement

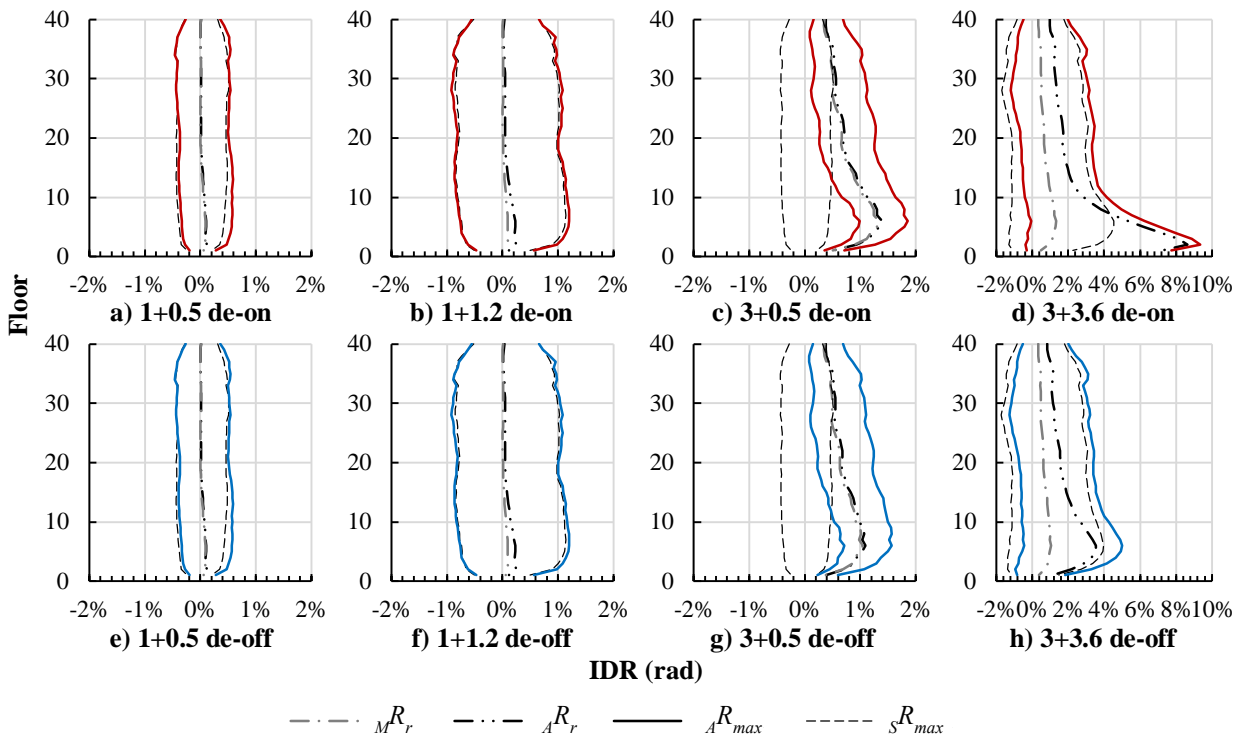


Fig. 6 – Floor Distribution of Response IDRs (JscaHachi)

plastic deformation, let alone further strength deterioration, the permanent deformation would last regardless considering the deterioration or not. For the case JscaHachi3+3.6, the difference was dramatically enlarged during the after event JscaHachi with $\phi=3.6$. The permanent displacement demand also largely increased for the de-on case (de-on) rather than the de-off one (de-off).

Floor distribution of main event residual IDR (M_{R_r}), after event residual IDR (A_{R_r}) and after event maximum IDR ($A_{R_{max}}$) at both plus-minus directions are shown in Fig. 6.

The maximum IDR of target model's virgin response under a single seismic input, which equivalent to the aftershock, ($S_{R_{max}}$) are also plotted in black dash line for comparing with the $A_{R_{max}}$. Overall, the $A_{R_{max}}$ at both plus-minus directions for all cases were shifted from the $S_{R_{max}}$. The shift amount at all floors roughly equals to M_{R_r} at the certain floor, respectively.

For the cases JscaHachi1+0.5 (Fig. 6a, e) and 1+1.2 (Fig. 6b, f), similar to the roof drift displacement response results shown in Fig. 5, no obvious difference can be confirmed between the de-on results and the de-off results. The $A_{R_{max}}$ slightly shifted from the $S_{R_{max}}$ to the direction which M_{R_r} occurred, which proved that the after-event response is different from the model's virgin response under a single-event input equivalent to the after event, because of the existence of main-event nonlinear response experience. In the case JscaHachi 1+1.2 (Fig. 6b, f), the plastic deformation also accumulated during the after event, as manifested in that the A_{R_r} were larger than M_{R_r} at lower floors.

For the case JscaHachi3+0.5 (Fig. 6c, g), difference in the main event residual IDR at about 1st-10th floors can be confirmed between the de-on result (Fig. 6c) and the de-off one (Fig. 6g). The maximum de-on M_{R_r} was about 0.4% rad larger than the de-off one. The shift of $A_{R_{max}}$ from the $S_{R_{max}}$ can also be confirmed obviously in both the de-on and de-off results. However, the permanent residual IDR did not increase for both the de-on and de-off cases, because of a weak after event input JscaHachi \times 0.5.

For the case JscaHachi3+3.6 (Fig. 6d, f), the difference between the de-on/de-off M_{R_r} were identical to the case JscaHachi3+0.5. However, the after-event $A_{R_{max}}$ and A_{R_r} were dramatically different between the de-on results (Fig. 6d) and the de-off ones (Fig. 6f). The largest $A_{R_{max}}$ of de-on case occurred at 2nd floor at + direction, different to the de-off one occurred at the 6th floor. The value of de-on largest $A_{R_{max}}$ reached 9.4%



rad, about twice of the de-off AR_{max} 's. The AR_r of de-on case, followed the floor distribution features of AR_{max} , occurred at 2nd floor with a value of 8.6% rad, about twice of the de-off AR_r 's. Such floor distribution and the sever values of AR_{max} and AR_r at the 1st and 2nd floors suggested that the model suffered a story collapse in the case deterioration considered. This story collapse phenomenon did not occur in the case deterioration ignored.

In addition, attention should be paid to draw such conclusions like that residual IDR or permanent deformation always increased during after events for all successive strong ground motion sequences. In this research, the main event and the after event were constructed by scaling one original wave. As a result, the main event and after event ground motions are sharing same periodic and phase characteristics. Thus, the main-event and after-event R_{max} or R_r tends to occur at similar directions.

3.3 A Prediction Approach for the After Event Maximum IDR

As mentioned above, the mainshock residual drift proved to play a vital role for the response of the model under successive ground motion sequences, just as what has been suggested by Ruiz-Garcia and Aguilar [13] that the mainshock residual drifts influenced the aftershock capacity of collapse, concluding from the aftershock IDA of a half-modeled 4-story SMRF. It goes without saying that the post-mainshock response starts from a start point that the residual drift has occurred. Here, we assume that the response features of the model would not change despite the main event response experience. Under this assumption, the only difference between the A-Response (the aftershock response of a deformed nonlinear system) and the S-Response (the virgin response of the same undamaged system subjected to an equivalent single event to the after event) was that A-Response starts from the residual deformation at the end of the main event. On the other hand, the S-Response starts from the original shape. The A-Response and S-Response would share the same response displacement amplitude.

If the assumption was true, A-Response could be predicted by the summation of S-Response deformation and the main event residual deformation. Specifically, the after event maximum IDR (AR_{max}) of a nonlinear system can be predicted by Eq. (1):

$$pAR_{max} = MR_r + sR_{max} \quad (1)$$

in which pAR_{max} stands for the prediction of AR_{max} , MR_r stands for the main event residual IDR, sR_{max} stands for the maximum IDR of the virgin response of the same undamaged system subjected to an equivalent single event to the aftershock.

The accuracy of the prediction of AR_{max} can be seen in the Fig. 7. The ratio of AR_{max} to the prediction value pAR_{max} at the floor where the 'real' AR_{max} occurred was between 30% except the case JscHachi3+3.6. The

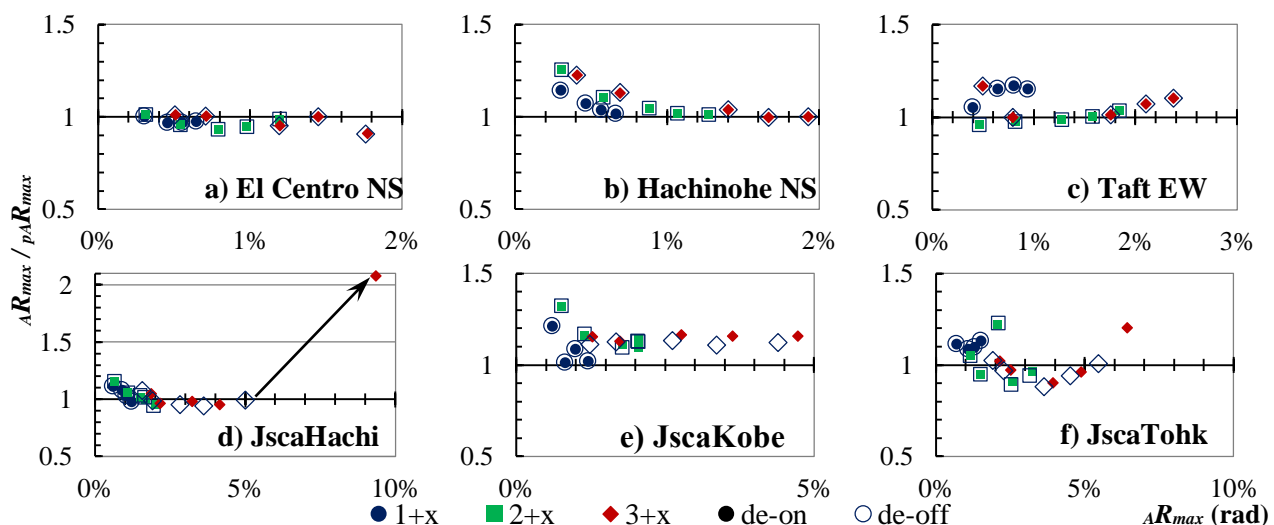


Fig. 7 – the Prediction Accuracy of AR_{max} for all Cases



ratio tends to increase in those cases which the abstract value of the response AR_{max} are smaller than 1%. The prediction largely underestimated the response in the case JscHachi3+3.6 (de-on). As introduced in **Section 3.2**, the value of AR_{max} was 9.4% rad, about twice of the prediction value pAR_{max} .

3.4 Response Details of the Case JscHachi3+3.6

To illustrate the reason for the difference on the model's de-on/off response under JscHachi3+3.6 and on the prediction accuracy for the AR_{max} , the predicted values pAR_{max} and the response AR_{max} at all floors of the model under the input case JscHachi3+3 and 3+3.6 are compared in Fig. 8. The pAR_{max} (dot line) has a good agreement with the AR_{max} under the case JscHachi3+3 (Fig. 8a, b). However, in the case JscHachi3+3.6, when the model considering deterioration, significant deformation can be confirmed by the value of AR_{max} (solid line) at 1st and 2nd floor. The predict underestimation for AR_{max} as motioned in **Section 3.3** can be confirmed at lower floors.

The comparison between the response IDR time history (solid line) under the input JscHachi3+3.6 and the prediction for the after-event time history (dot line) at the 1st floor and the 40th floor can be seen in Fig. 9. The prediction of the response IDR time history was made by adding MR_r to the undamaged model's virgin response IDR time history subjected to a single event. The single event at this case refers to JscHachi3.6. While the deterioration was ignored in the model, the response IDR follows the prediction well both at the top and the bottom floor. While the deterioration was considered in the model, the response IDR time history at the 1st floor deviated from the prediction one after the IDR was larger than 2% rad and obviously accumulated to one side, ended with roughly 5% rad difference between the value of response IDR and the prediction one's.

The hysteric records of bending moment-curvature ($M-\phi$) and normalize axial force-bending moment ($N-M$) of 1st floor columns' bottom hinge section were compared under those two mentioned circumstances, in Fig. 10. The Axial Force has been normalized by the yield axial load N_y and the bending moment has been normalized by the bending moment capacity M_p . C1 stands for the left side (- direction side) column, C3 stands for the center column, C5 stands for the right side (+ direction side) column.

As shown in Fig. 10b, d, when the members' deterioration ignored, only slightly difference of the $M-\phi$ and $N-M$ records can be confirmed between the A-Response and the S-Response. The considerable reason for

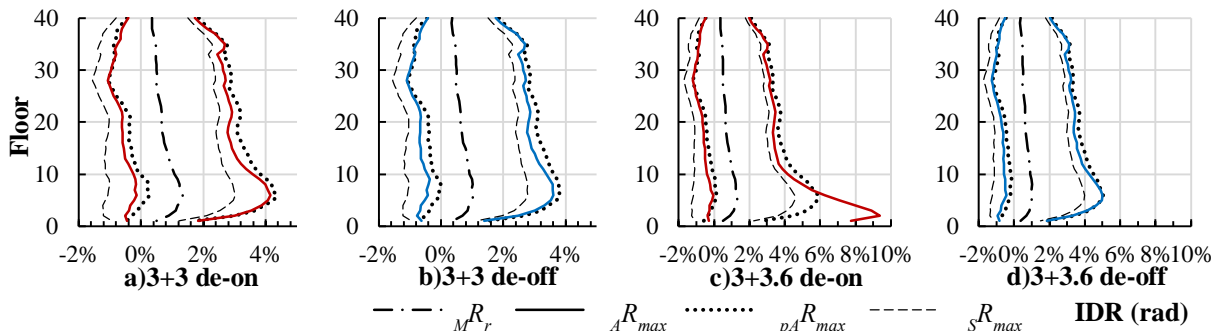


Fig. 8 – Comparison of pAR_{max} with AR_{max} (JscHachi 3+3/3+3.6)

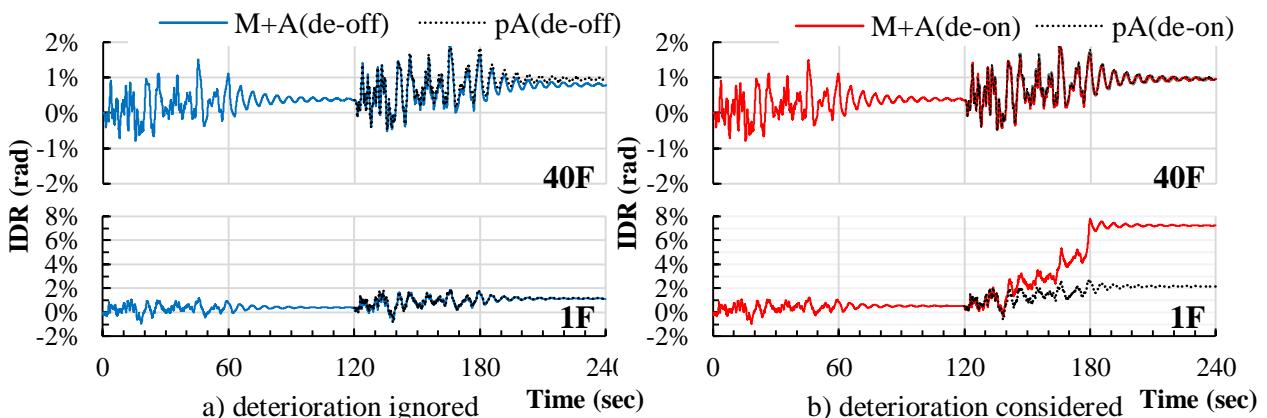


Fig. 9 – Time History of IDR at 1F and 40F (JscHachi3+3.6)

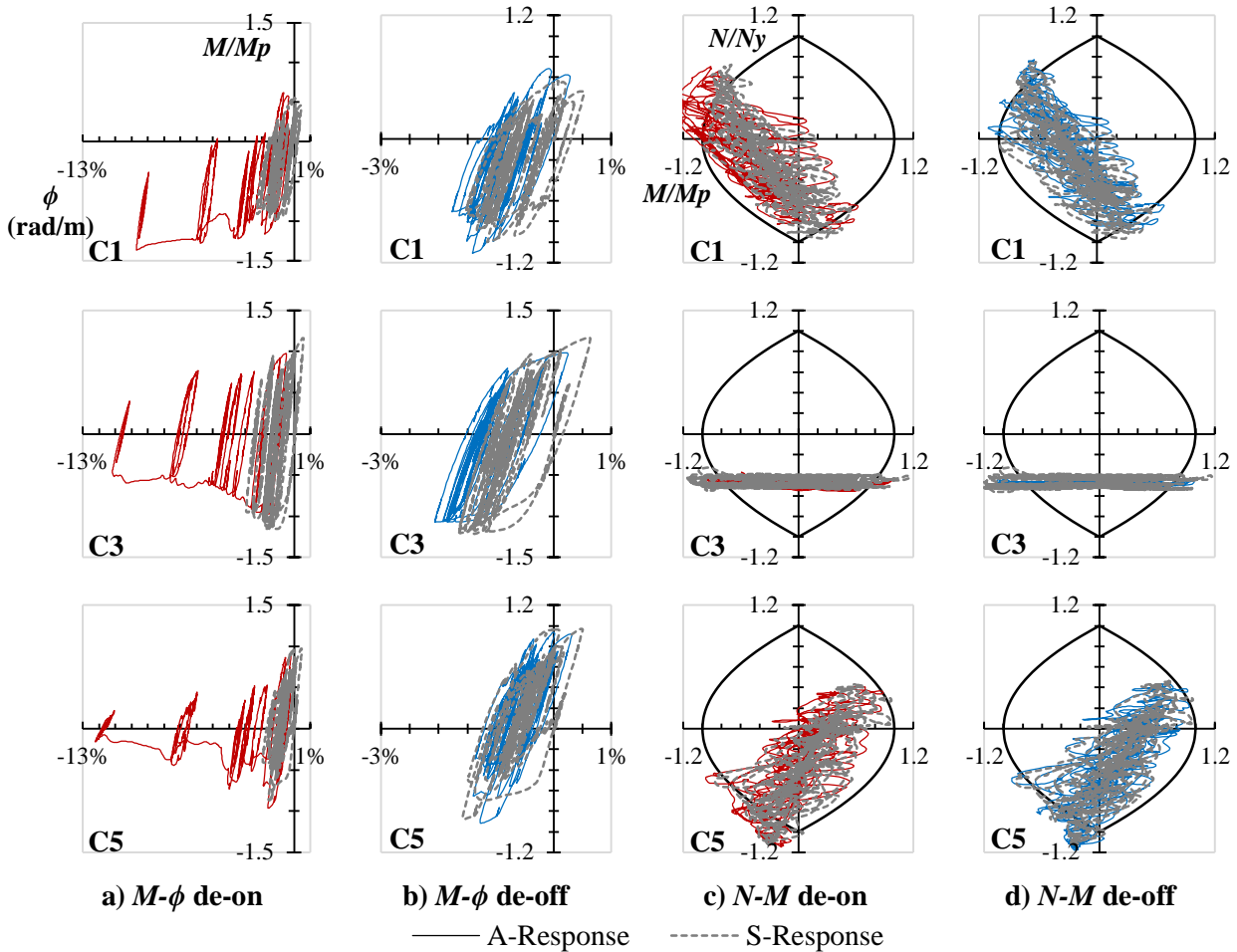


Fig. 10 – Response History of M - ϕ and N - M (JscaHachi3+3.6)

such difference could be the main-event deformation and the main-event strain-hardening experience of the model. However, the deterioration effect has been ignored in this case. Similarity between the A-Response and S-Response M - ϕ / N - M records could be an evidence for the good agreement of the after-event prediction as shown in Fig. 8d and Fig. 9a.

When the deterioration considered, as shown in Fig. 10a, c, obvious difference between the A-Response and the S-Response can be confirmed. To be more specific, in the A-Response M - ϕ response history (Fig. 10a), curvature of all the three columns' bottom hinge accumulated to one direction. The initial deterioration experience of the model influenced the A-Response. However, such deterioration effects were not evident in the S-Response, which contributed to the underestimation for the maximum deformation (or AR_{max}) and the permanent deformation (or AR_r) demands.

The strength deterioration effect performed asymmetrically on C1, C3 and C5. For C3 and C5, the bending strength deterioration can be confirmed. For C1, the strength increased while curvature accumulating. The considerable reason for this asymmetric can be found in the N - M records (Fig.10 c). Varying axial load observed in the N - M records of C1 and C5, while the axial force kept a certain level for C3. Specifically, for C1, the combination of large tensile axial force and bending moment load, which larger than the S-Response one, drive C1 to its ultimate capacity. For C3, though the axial load kept at a certain level, the strength deterioration can be confirmed at the started part of A-Response. This initial damage caused by the main event lead to the decreasing on bending moment resistance and the accumulation of curvature. For C5, the noticeable compression axial load combined with bending moment, which larger than the S-Response, accumulated the strength deterioration of C5. The curvature deformation accumulating along with the bending moment resistant decreasing. However, these severe nonlinear behaviors, considered as the result of the main event residual



deformation and the main-event strength deterioration experience, cannot be reflected by the S-Response records.

4. Conclusions

The response of a high-rise SMRF model subjected to the artificial successive ground motions with various intensity combinations were calculated. The influence of members' strength deterioration on the after-event response was evaluated. The after-event maximum IDR (${}_A R_{max}$) and residual IDR (${}_A R_r$) were mainly concerned in the discussion. Several conclusions and inferences can be drawn from this study:

1. The after event response deformation of the model are largely influenced by the main event residual deformation for all cases, despite the consideration on the deterioration. The influence features of the strength deterioration depend on the intensity combination of main event and after event;

2. A prediction approach for the after event response IDR was proposed, based on the assumption that the after-event response of a plastically deformed model keeps the same response feature with an undamaged one. The accuracy of this approach is relatively acceptable for most input cases except the case set: JscaHachi3+3.6, in which unexpected story collapse occurred while considering the structural members' strength deterioration;

3. From the analysis of the case JscaHachi3+3.6, the main event residual IDR and the damage, in terms of the strength deterioration, are considered responsible for the severe nonlinear behavior in the aftershock of the strong sequences. The prediction approach for this case leads to a risky underestimation. In this case, the influence performed asymmetrically in the 1st floor columns.

This research has to be considered as preliminary. As all of the steel structural members were high ductile members (Rank FA), the story collapse only occurred in case JscaHachi3+3.6. It can be anticipated that story collapse might occur under lower-intensity MSAS for the SMRFs constructed by relatively lower ductile members (Rank FB). Further investigations are needed on the models constructed by Rank FB members.

5. Acknowledgements

The Building Center of Japan (BCJ) and Japan Structural Consultants Association (JSCA) are specifically acknowledged for provided the ground motion records used in this study.

6. References

- [1] Tsai KC, Hsiao CP, Bruneau M (2000): Overview of Building Damages in 921 Chi-Chi Earthquake. *Earthquake Engineering and Engineering Seismology*, **2** (1), 93-108.
- [2] Architectural Institute of Japan (AIJ) (2011): *Preliminary Reconnaissance Report of the 2011 Tohoku-Chiho Taiheiyō-Oki Earthquake*. AIJ, 1st edition. (in Japanese)
- [3] Architectural Institute of Japan (AIJ) (2018): *Report on the Damage Investigation of the 2016 Kumamoto Earthquakes*. AIJ, 1st edition. (in Japanese)
- [4] Amadio C, Fragiacomano M, Rajgelj S (2003): The effects of repeated earthquake ground motions on the non-linear of SDOF systems. *Earthquake Engineering & Structural Dynamics*, **32**, 291-308.
- [5] Hatzigeorgiou GD, Beskos DE (2009): Inelastic displacement ratios for SDOF structures subjected to repeated earthquakes. *Engineering Structures*, **31**, 2744-2755.
- [6] Hatzigeorgiou GD (2010): Behavior factors for nonlinear structures subjected to multiple near-fault earthquakes. *Computers and Structures*, **88**, 309-321.
- [7] Zhai C, Wen W, Ji D, Li S (2015): The influences of aftershocks on the constant damage inelastic displacement ratio. *Soil Dynamic and Earthquake Engineering*, **79**, 186-189.
- [8] Yaghmaei-Sabegh S, Ruiz-Garcia J (2016): Nonlinear response analysis of SDOF systems subjected to doublet earthquake ground motions: A case study on 2012 Varzaghan-Ahar events. *Engineering Structures*, **110**, 281-292.



- [9] Rinaldin G, Amadio C, Fragiaco M (2017): Effects of seismic sequences on structures with hysteretic or damped dissipative behavior. *Soil Dynamic and Earthquake Engineering*, **97**, 205-215.
- [10] Fragiaco M, Amadio C, Macorini L (2004): Seismic response of steel frames under repeated earthquake ground motions. *Engineering Structures*, **26**, 2021-2035.
- [11] Li Q, Ellingwood BR (2007): Performance evaluation and damage assessment of steel frame buildings under main shock-aftershock earthquake sequences. *Earthquake Engineering & Structural Dynamics*, **36**, 405-427.
- [12] Ruiz-Garcia J, Negrete-Manriquez JC (2011): Evaluation of drift demands in existing steel frames under as-recorded far-field and near-fault mainshock-aftershock seismic sequences. *Engineering Structures*, **33**, 621-634.
- [13] Ruiz-Garcia J, Aguilar JD (2015): Aftershock seismic assessment taking in to account postmainshock residual drifts. *Earthquake Engineering & Structural Dynamics*, **44**, 1391-1407.
- [14] Hatzigeorgiou GD, Liolios AA (2010): Nonlinear behaviours of RC frames under repeated strong ground motions. *Soil Dynamics and Earthquake Engineering*, **30**, 1010-1025.
- [15] Ruiz-Garcia J, Marin MV, Teran-Gilmore A (2014): Effects of seismic sequences in reinforced concrete frames buildings located in soft-soil sites. *Soil Dynamics and Earthquake Engineering*, **63**, 56-68.
- [16] Morfidis K, Kostinakis K (2017): The role of masonry infills on the damage response of R/C buildings subjected to seismic sequences. *Engineering Structures*, **131**, 459-476.
- [17] Shen J, Akbas B, Seker O, Doran B, Wen R, Uckan E (2015). Seismic axial loads in steel moment resisting frames. *International Journal of Steel Structures*, **15**, 375-387.
- [18] Kim M, Araki Y, Yamakawa M, Tagawa M, Ikago K (2009): Influence of P-Delta Effect on Dynamic Response of High-rise Moment-Resisting Steel Buildings Subjected to Extreme Earthquake Ground Motions. *Journal of Structural and Construction Engineering (Transactions of AIJ)*, **74**(644): 1861-1868. (in Japanese)
- [19] Bai Y, Shi Y, Deng K (2016): Collapse Analysis of High-rise Steel Moment Frames Incorporating Deterioration Effects of Column Axial Force-Bending Moment Interaction. *Engineering Structures*, **127**, 402-415.
- [20] Vamvatsikos D, Cornell CA (2002): Incremental Dynamic Analysis. *Earthquake Engineering and Structural Dynamics*, **31**(3): 491-514.
- [21] Kawano A, Warner RF (1995): Nonlinear analysis of the time-dependent behaviour of reinforced concrete frames. *Research Report No. R125*. Department of Civil and Environmental Engineering, the University of Adelaide.
- [22] Kato B, Akiyama H, Yamanouchi H (1978): Experimental studies on the plastic deformation capacity of box sectional members, (Part 3. For cold-formed box sectional members). *Summaries of technical papers of annual meeting Architectural Institute of Japan*, **48**: 937-938. (in Japanese)
- [23] Meng L, Ohi K, Takanashi K (1992): A simplified model of steel structural members with strength deterioration used for earthquake response analysis. *Journal of Structural and Construction Engineering (Transactions of AIJ)*, **437**(0): 115-124. (in Japanese)
- [24] Popovics S (1973): A numerical approach to the complete stress-strain curve of concrete. *Cement and Concrete Research*, **3**(5), 583-599.
- [25] Fujii M, Bai Y, Egashira S, Kawano A, Matsuo S (2013): Damage characteristics of existing super high-rise steel frame buildings and CFT frame buildings under severe earthquake ground motions. *Journal of structural engineering. B*, **59B**, 181-190. (in Japanese)